Signal Processing Approach to Detect Non-Metallic Targets for Through Wall Imaging Using UWB Antenna

Sajjad Ahmed[1,2], Fawad Salam Khan[3], Imran Khan Keerio[4], Arslan Ahmed[1,2], Sarfraz Ahmed[5]
[1]Faculty of Electrical and Electronic Engineering, University Tun Hussein Onn Malaysia (UTHM), Johor, Malaysia
[2]Faculty of Engineering, The University of Larkano, (TUL), Larkana, Sindh, Pakistan
[3]Department of Creative Technologies, Faculty of Computing and AI, Air University Islamabad, Pakistan
[4]Departement of Computer Science, Sindh Madressatul Islam University, Karachi Pakistan
[5]Department of Telecommunication Engineering, Quaid-e-Azam University of Engineering, Science and Technology (QUEST) Nawabshah, Pakistan
*Correspondence: sajjadbhatti@uolrk.edu.pk

Citation | Ahmed. S, Khan. F. S, Keerio. I. K, Ahmed. A, Ahmed. S, "Signal Processing Approach to Detect Non-Metallic Targets for Through Wall Imaging Using UWB Antenna", IJIST, Vol. 06 Issue. 04 pp 2195-2208, Dec 2024
Received | Nov 26, 2024 **Revised |** Dec 18, 2024 **Accepted |** Dec 24, 2024 **Published |** Dec 26, 2024.

This paper presents a signal-processing approach aimed at detecting non-metallic targets through walls using an Ultra-Wideband (UWB) antenna configuration. Through-wall imaging holds significant importance in various fields including security, surveillance, and search and rescue operations. The proposed methodology involves the utilization of the UWB Antipodal Vivaldi antenna (AVA), known for its wide bandwidth and high-resolution imaging capabilities. The study focuses on the detection of non-metallic targets using signal processing techniques. A through-wall simulation model utilizing a UWB AVA has been developed in CST Microwave Studio. This model generates received signals in the time domain for through-wall target detection, which are subsequently processed using signal processing techniques to produce 2D images.

Keywords. Signal Processing; Through-Wall Imaging; Non-Metallic Targets; Time Domain; UWB; AVA; CST.

Introduction:

Through-wall object detection and imaging have gained significant attention due to their potential applications in fields such as search and rescue operations, surveillance, and security [1][2][3]. UWB technology finds applications in communication systems, radar systems, and imaging [4][5][6], including Ground Penetrating Radar (GPR), diagnostic medical imaging, and through-wall detection of hidden non-metallic objects [7][8][9]. Researchers have proposed various methodologies and techniques for through-wall object detection using UWB systems. Common approaches include time-domain and frequency-domain signal processing. The UWB signal, characterized by short pulses separated in time, enhances spatial resolution and short-range capability. When applied in antenna systems, the increased bandwidth allows for better target information acquisition, improving overall performance. Antennas act as the interface between the system and the environment [10]. They transmit UWB signals into the surrounding space and receive reflected signals from targets behind walls.

The antenna's design and characteristics directly impact the radiation pattern, polarization, and bandwidth of both transmitted and received signals, significantly affecting the overall system performance. In UWB-TWI systems, antennas play a critical role in maximizing signal penetration while minimizing losses due to wall absorption and scattering [11]. Antennas with appropriate radiation characteristics and polarization facilitate efficient signal propagation through various wall materials, enhancing detection sensitivity and range. The UWB antipodal Vivaldi antenna, designed for TWI systems, boasts wide bandwidth, enabling efficient transmission and reception of UWB signals. This capability facilitates high-resolution imaging and accurate detection of targets concealed behind walls [12]. The antenna's design minimizes dispersion effects, enhancing precision in TWI applications. Its directional radiation patterns improve spatial coverage and sensitivity, enhancing signal penetration and target detection performance. Additionally, its compact size and low profile make it suitable for portable and lightweight TWI systems [13]. The antenna's simplicity and broadband nature ensure consistent performance across diverse operating conditions. However, despite significant progress, challenges persist in TWI using UWB antipodal Vivaldi antennas. Multipath propagation, wall penetration losses, and signal attenuation degrade received signal quality, resulting in reduced detection range and accuracy. Environmental factors, such as building materials and structural interference, further complicate reliable through-wall sensing. Addressing these challenges necessitates interdisciplinary research efforts spanning electromagnetics and signal processing.

This paper presents the development of a simulation model developed for through-wall scenarios employing a UWB AVA antenna within CST MWS. The simulation model leverages the Finite Integration Technique (FIT) method to accurately replicate the target response within the time domain signal. Additionally, the paper delves into the design considerations essential for the antenna system and investigates the foundational principles of UWB-TWI.

Methodology:

The methodology of this paper involves the design of an UWB AVA, the development of a through-the-wall simulation model, and the application of signal processing techniques to generate target images. Figure 1 shows the flow chart of the TWI simulation system implemented in this study.

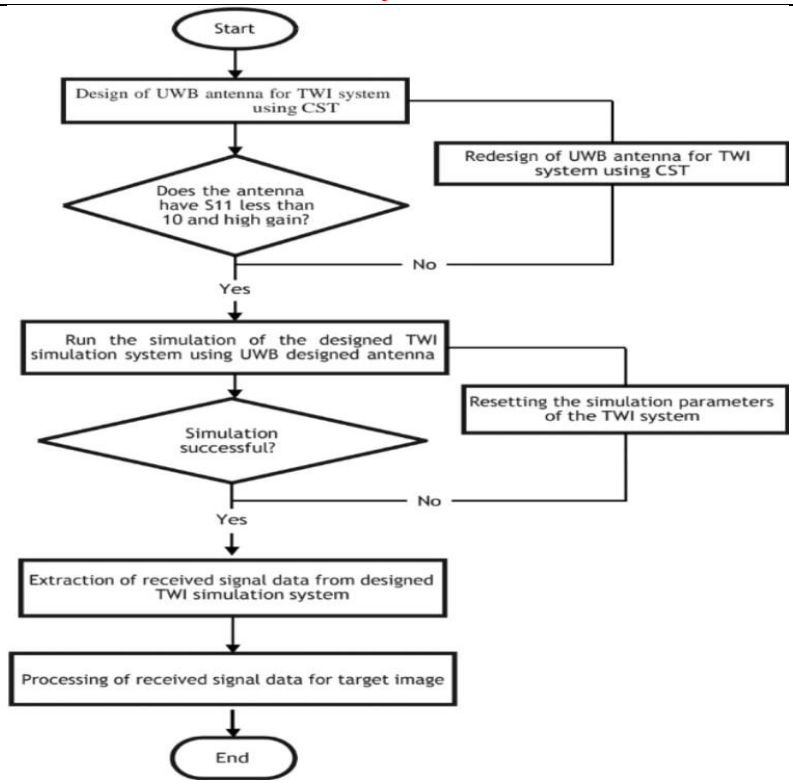

Figure 1. Flow chart of TWI simulation system setup

Objectives of the Study:

- To design and implement a signal-processing methodology for detecting non-metallic targets through walls using an UWB antenna configuration.
- To utilize the UWB AVA for its wide bandwidth and high-resolution imaging capabilities in detecting non-metallic targets.
- To create a through-wall simulation model in CST Microwave Studio that accurately represents the detection process and generates time-domain signals for further analysis.
- To process the received signals using advanced signal-processing techniques to generate 2D images, enabling clear visualization of non-metallic targets behind walls.

Novelty of the Study:

The research introduces a novel algorithm to form 2D images of objects from the received signals, representing a significant advancement in the field of through-wall imaging for applications such as security and search-and-rescue operations.

UWB Modified Antipodal Vivaldi Antenna (MAVA) Design:

The MAVA antenna is designed using a Rogers 5880 substrate (1.58 mm thick) and features a 50 Ω microstrip line with a width (Wc) of 4.58 mm. The deliberate choice of Rogers 5880 material is due to its favorable tangential loss properties, contributing to high gain [14]. The MAVA design incorporates two identical elliptic curves from references [15][16]. The antenna consists of two essential components: the feed line and the radiating flared wings. The elliptical slot design in an antipodal Vivaldi antenna plays a crucial role in influencing both impedances matching and the radiation pattern. For impedance matching, the gradual tapering of the elliptical slot ensures a smooth transition for electromagnetic waves, minimizing reflections and enabling efficient transmission. This design feature significantly improves impedance matching over a wide frequency range, while also enhancing the bandwidth by lowering the cut-off frequency, allowing the antenna to perform effectively across a broader spectrum. Regarding the radiation pattern, the elliptical slot helps achieve a more directional radiation profile by focusing the radiated energy in a specific direction, thereby improving the

antenna's directivity. Additionally, it contributes to reducing side lobes, which minimizes unwanted radiation and results in a cleaner, more focused main lobe. These characteristics collectively enhance the antenna's overall performance. To enhance performance, the MAVA antenna employs a slot structure [17]. Each MAVA flare has a central circular slot (CS), along with seven elliptical slots (ES) of varying dimensions. To achieve optimal performance in an antipodal Vivaldi antenna (AVA), the Parameter Sweeping technique is employed to fine-tune key dimensions such as length, slot width, and feeding structure. This method involves systematically varying one parameter at a time within a defined range while keeping the others fixed. By doing so, the influence of each parameter on the antenna's performance can be effectively analyzed and understood. The design process involved meticulous optimization of dimensions using CST Microwave Studio®. CST provides a powerful platform for TWI simulations, inherent limitations and errors necessitate careful validation. By addressing discrepancies through experimental comparisons and iterative refinements, the reliability and applicability of the simulation model can be enhanced. This ensures that the results from the CST model are credible and applicable to real-world scenarios. Table 1 provides detailed dimensions in millimeters, and Figure 2 visually depicts the antenna layouts: (a) shows the geometrical arrangement, while (b) presents the CST layout.

Table 1. Dimensions of MAVA

Parameters	Value (mm)
W	60.90
L	66.10
D	27
Wa	53
Wc	4.58
We	11.78
CS (L &W)	5
ES (2-6) W	5
ES (1 & 7) W	5.80

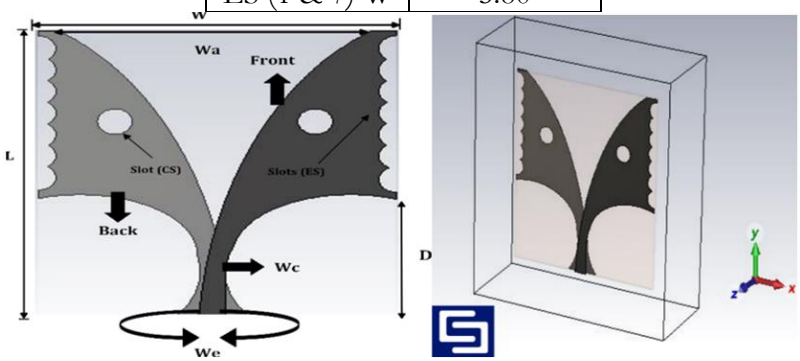

Figure 2. MAVA antenna layout, (a) Geometric layout, (b) CST layout

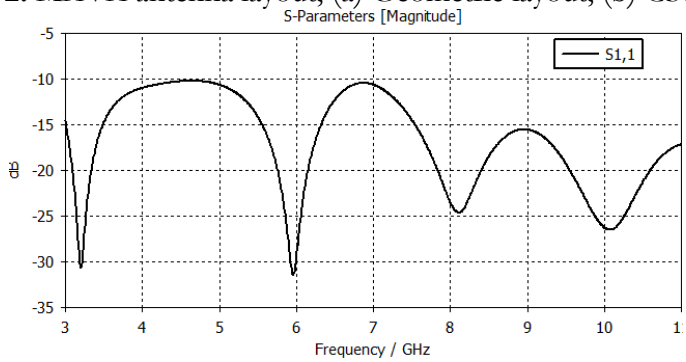

Figure 3: Reflection coefficient S_{11} of MAVA

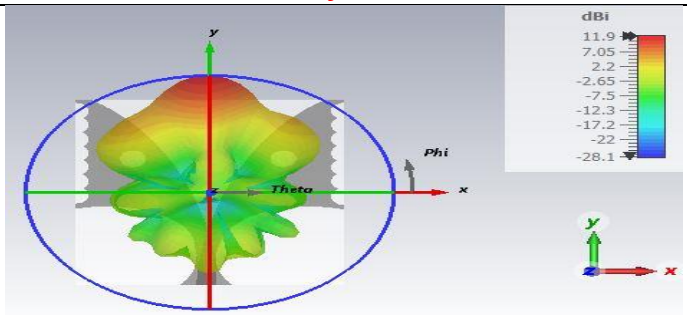

Figure 4. 3D far-field radiation pattern of the MAVA

Table 2. S_{11} of MAVA

Frequency (GHz)	S_{11} (dB)
3	-13.71
3.5	-15.75
4	-10.83
4.5	-10.21
5	-10.24
5.5	-13.53
6	-29.35
6.5	-12.26
7	-10.879
7.5	-14.68
8	-25.26
8.5	-18.11
9	-14.26
9.5	-17.20
10	-23.34
10.5	-21.29

The Reflection coefficient (S_{11}) measures the amount of electromagnetic energy reflected by an antenna due to impedance mismatches or other factors. For optimal performance, an acceptable S_{11} value is below -10 dB. In the case of the MAVA antenna, the simulated S_{11} (shown in Figure 3) falls below this threshold, indicating excellent impedance matching. Table 2 shows S11 values for different frequencies, with values less than -10 dB considered acceptable for system performance. All frequencies meet the S11 < -10 dB criterion, but performance varies across the range. Low S11 values indicate excellent impedance matching for frequencies like 6 GHz, 8 GHz, and 10 GHz. However, frequencies closer to -10 dB, like 4 GHz, 4.5 GHz, and 5 GHz, show less optimal performance compared to others. Additionally, Figure 4 presents a 3D far-field radiation pattern of the MAVA at higher frequencies, revealing both the intensity and direction of emitted electromagnetic waves. Lastly, Figure 5 demonstrates the simulated gain of the MAVA in the H-plane at 10 GHz, achieving an impressive value of approximately 11.9 dB. Overall, the proposed antenna exhibits advantageous radiation properties.

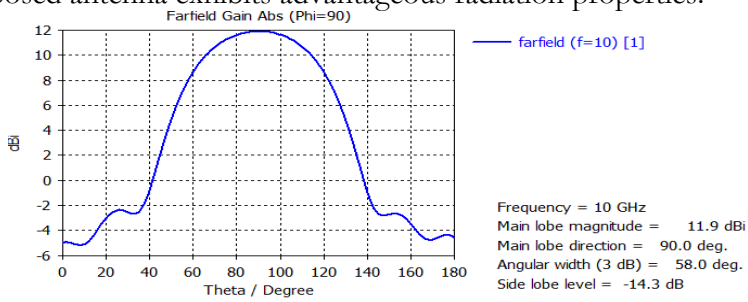

Figure 5. Simulated gain of MAVA in H-plane at 10 GHz

Figure 6 illustrates the simulated gain characteristics of the MAVA antenna across the frequency range from 3 GHz to 10 GHz. Notable observations include gains of 3 dB at 3 GHz, 6.2 dB at 4 GHz, 7.5 dB at 5 GHz, 9.2 dB at 6 GHz, 10.3 dB at 7 GHz, 9 dB at 8 GHz, 10.2 dB at 9 GHz, and 11.9 dB at 10 GHz. The simulated peak gain occurs at 10 GHz, reaching approximately 11.9 dB.

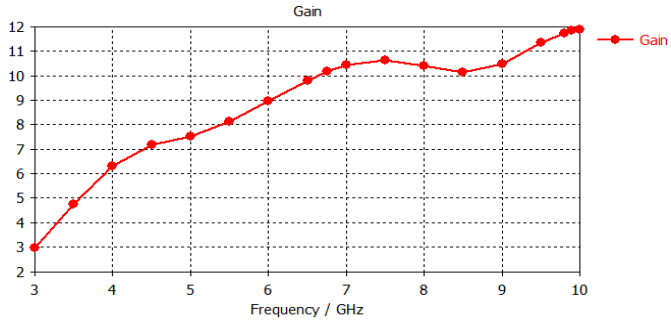

Figure 6. Simulated gain of MAVA (3-10 GHz)

Through Wall Simulation Model:

In the wall scanning model using the Synthetic Aperture Radar (SAR) approach, the first and third layers are composed of free space. Figure 7 illustrates this setup, where a single MAVA antenna is placed at a specific location. The antenna transmits and receives signals, then moves to the next location, repeating this process along the wall's axis. The second layer represents the wall itself, with a thickness denoted as dw and a permittivity represented by εw.

When electromagnetic waves interact with a target object (such as wood or rubber) behind a wall, the interaction depends on the material properties of both the wall and the target object. These properties, such as permittivity, permeability, and conductivity, influence how the waves are reflected, refracted, absorbed, and scattered. Wall material, such as concrete, brick, or drywall, significantly influences signal interaction by reflecting, refracting, attenuating, and causing multipath effects. Higher permittivity materials reflect more energy, while higher conductivity reduces signal strength. The wave's interaction with the target depends on its material properties. Wood has low conductivity, absorbing energy, and moderate absorption. Rubber has higher permittivity, low conductivity, and strong damping properties, causing wave deformation. The wall and target material together affect the received signal, causing signal degradation, frequency dependence, and time delay. Wall attenuation reduces signal strength, while target properties affect reflection, absorption, or scattering. Higher frequencies provide better resolution but suffer attenuation. Non-metallic targets like wood and rubber are difficult to detect due to their low reflectivity compared to metals. They are more detectable due to their increased permittivity and conductivity. Moisture content also affects their interaction, making wet wood more detectable. Techniques like time-domain analysis and 2D imaging extract valuable information from attenuated and scattered signals.

The dielectric constant (εr) and loss tangent (δ) of materials such as concrete, rubber, and wood vary based on frequency, material composition, and environmental factors like moisture content. For concrete walls, the dielectric constant (εr) ranges from 4.5 to 10, with lower values for dry concrete and higher values for wet concrete. The loss tangent (δ) for concrete ranges from 0.02 to 0.5, being highly dependent on humidity and frequency. Rubber has a dielectric constant (εr) of 2.5 to 4, depending on the type, such as natural or synthetic rubber. Its loss tangent (δ) ranges from 0.02 to 0.2, with higher values typically found in synthetic rubber with additives. Wood exhibits significant variation due to moisture, with the dielectric constant (εr) of dry wood ranging from 2 to 6, while wet wood ranges from 10 to 20. The loss tangent (δ) for dry wood is between 0.01 and 0.1, whereas wet wood shows a higher range of 0.2 to 0.5, as moisture substantially impacts these values.

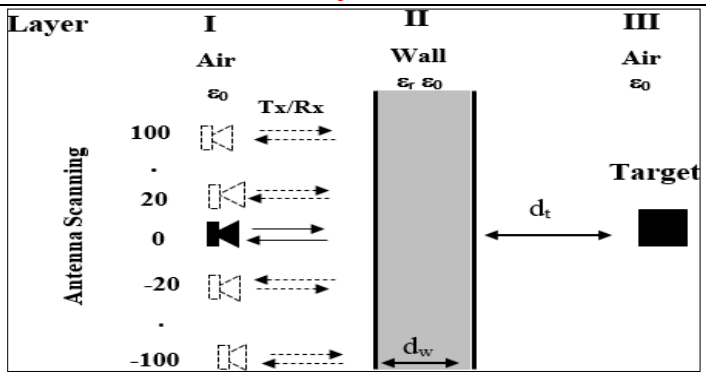

Figure 7. Through wall simulation Model

The methodology for simulating TWI systems using CST software encompasses several essential steps:

- **Model Setup**: The simulation initiates with configuring the model within the CST software. This entails defining the geometry and material properties of the components involved, including the MAVA antenna, concrete wall, and non-metallic objects (wood and rubber).
- **Antenna Configuration:** The MAVA antenna transmits electromagnetic signals in a monostatic configuration, where the same antenna serves for both transmission and reception. Parameters such as frequency, polarization, and radiation pattern are appropriately configured for the simulation.
- **Wall Parameters:** The concrete wall is modeled with specific dimensions - 300 x 300 mm^2 in size and 300 mm thickness. The distance between the antenna and the wall is set at 200 mm.
- **Target Placement:** The wood and rubber representing the target behind the wall, is introduced into the simulation model. Its dimensions (100 x 100 mm^2 and 20 mm thickness) and position relative to the wall are specified. The targets are placed at varying distances (d_t) from the wall, 0.2 m, and 0.4 m to simulate diverse scenarios.
- **Simulation Execution:** With all parameters set, the simulation is executed. Maxwell's equations are solved to simulate electromagnetic wave propagation through the environment, encompassing interactions with the wall and target object.
- **Data Analysis:** Post-simulation, collected data such as reflected signals are analyzed to extract pertinent information. This analysis may include target presence detection, distance estimation from the wall, and reconstruction of a target image behind the wall.
- **Validation**: Simulation results are validated against established theoretical principles or experimental data to ascertain the accuracy and reliability of the model.

By adhering to this methodology, the performance of TWI systems can be effectively simulated and evaluated using CST software.

Signal Processing for Target Imaging:

Figure 8 shows the time-domain transmitted signal of the MAVA antenna in the UWB frequency range (from 3 GHz to 10 GHz). This signal, resembling a Gaussian pulse, serves as the incident wave source in CST MWS software. In Figure 9, we observe the time-domain signal received by the same MAVA antenna as it interacts with the air, also within the UWB frequency range.

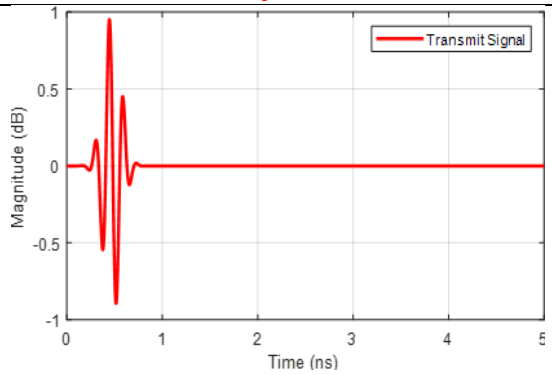

Figure 8: Transmitted signal of MAVA antenna

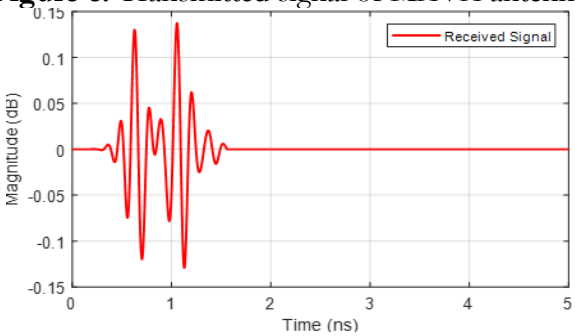

Figure 9. Received signal of MAVA antenna

This methodology outlines a systematic approach for developing an image of targets behind a wall using scanning techniques:

- **Scanning Setup:** Position an antenna to scan the wall at various positions, covering a wide area from 0 to both positive and negative positions.
- **Antenna Positioning:** Place the antenna horizontally to maximize wall coverage and capture potential signals reflected from the object behind it.
- **Scanning Positions:** Utilize 11 strategically chosen scanning positions with a 20 mm gap between each, minimizing blind spots.
- **Target Placement:** Position rubber and wood targets in the middle behind the wall for optimal scanning and varied reflection angles.
- **Data Collection:** Collect signal data as the antenna scans, including intensity and direction information.
- **Image Development:** The antenna collects data on signals it receives, including the intensity and direction of reflected signals from the object behind the wall at different positions.

To detect and image a small metal object located behind a wall at a distance of 0.2 m, we analyze received signals from three scanning positions. In Figure 10(a), the MAVA antenna's signals at the 0-scanning position reveal variations between 0.6-1.1 ns (antenna reflections) and 2.4-2.5 ns (wall reflections). Variations between 3.83-3.95 indicate scattered reflections from the metal object. Figures 10(b) and 10(c) show received signals at scan positions 100 and -100, respectively, without object reflections only antenna and wall reflections. Successful target detection involves additional signal processing to generate two-dimensional images from the dataset collected across 11 scanning positions (ranging from 100 to -100).

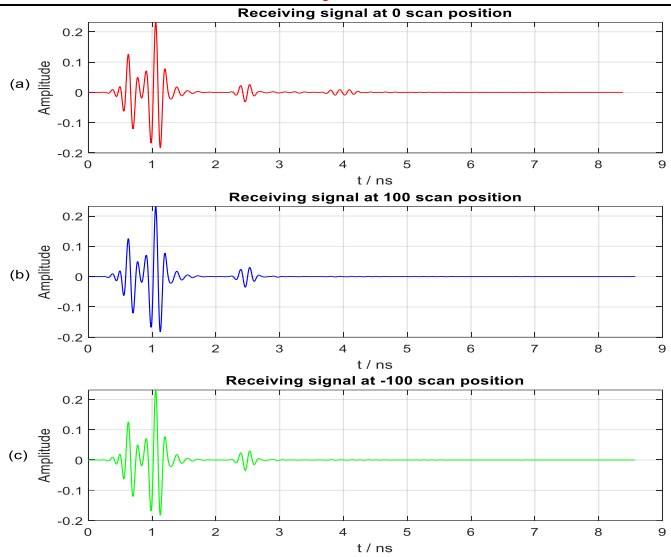

Figure 10. Receiving signals for rubber detection at 0.2 m (a) 0 scan position (b) 100 scan position (c) -100 scan position

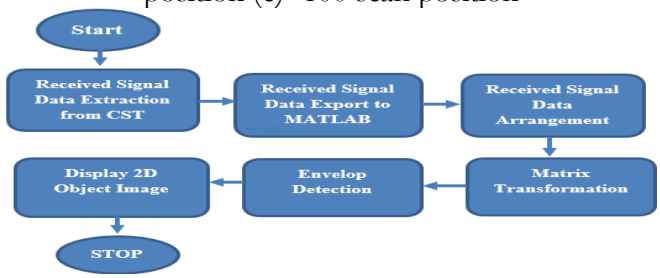

Figure 11. Flow chart for formation of 2d image of an object using signal processing techniques

Figure 11 presents a flowchart outlining the process of forming an object image using signal processing techniques:

- **Data Extraction:** Extract the dataset of received signals from 11 scanning positions (ranging from 100 to -100) using CST MWS.
- **Export and Processing:** Export the received signal data in CSV format for processing in MATLAB. Develop a dedicated program for further analysis.
- **Position Organization:** Organize the received signal data based on the MAVA antenna's scanning positions.
- **Matrix Transformation:** Apply a matrix transformation to generate a 2D image of the object.
- **Envelope Detection:** Employ envelope detection as a signal processing technique to enhance image quality.
- **Display Result:** Conclude the process by displaying the resultant image.

Envelope detection is a signal processing technique that extracts the amplitude envelope of a modulated signal, enhancing image quality in TWI by improving target detectability and reducing noise. Envelope detection reduces noise and artifacts by smoothing rapid oscillations in the received signal, focusing on dominant components like target reflections. It extracts amplitude variations for target detection and imaging, especially when the signal is modulated or contains higher-order reflections. The technique enhances contrast between the target and background, making the target more distinguishable. Envelope detection simplifies processing by providing a clear representation of the signal's intensity over time. Time-domain deconvolution and frequency-domain processing are two techniques used in signal analysis. Time-domain deconvolution corrects for multipath effects and distortions, providing sharper

resolution. It is computationally intensive and sensitive to noise, but less robust than envelope detection. Frequency-domain processing transforms signals into the frequency domain and analyzes spectral components for information extraction. It allows sophisticated filtering and analysis but requires additional computational steps and may struggle with non-stationary signals or rapid time-domain variations. It offers higher flexibility for detailed analysis but lacks the simplicity and directness of envelope detection for enhancing raw amplitude contrast in time-domain imaging.

Result and Discussion:

Figure 12 shows a 2D image of a rubber object located behind a wall at a distance of 0.2 meters. The y-axis represents the downrange where the target becomes visible at the same distance, while the x-axis illustrates the cross-range relative to the scanning antenna positions.

To detect the presence of a rubber object behind a concrete wall at a distance of 0.4 meters, we analyze received signals at three scanning positions. These positions include 0 as the central point, with 100 and -100 representing the upper and lower scanning positions, respectively. In Figure 13(a), the observed signal variation between 0.6-1.1 ns is attributed to antenna reflections, while the variation around 2.4 to 2.5 ns corresponds to wall reflections. Finally, the variation between 5.25 ns and 5.45 ns corresponds to the target. Figures 13(b) and 13(c) display received signals at scan positions 100 and -100, respectively. In these situations, object reflections are not present; only reflections from the antenna and wall are visible, consistent with the description in Figure 13(a). After successfully detecting the target, the received signal dataset from 11 scanning positions (ranging from 100 to -100) undergoes further processing using signal processing techniques to create two-dimensional images of the target.

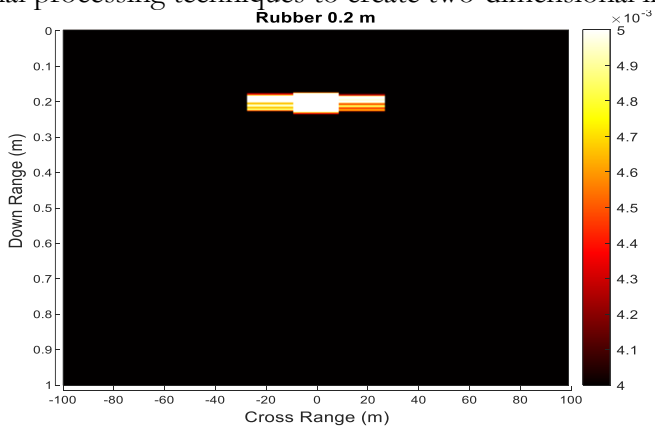

Figure 12. A 2D image depicts a rubber target situated 0.2 meters down range behind a wall

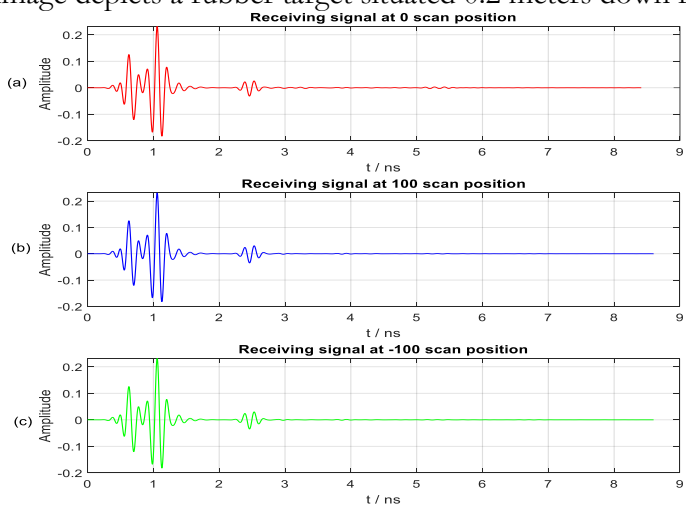

Figure 13. Receiving signals for rubber detection at 0.4 m (a) 0 scan position (b) 100 scan position (c) -100 scan position

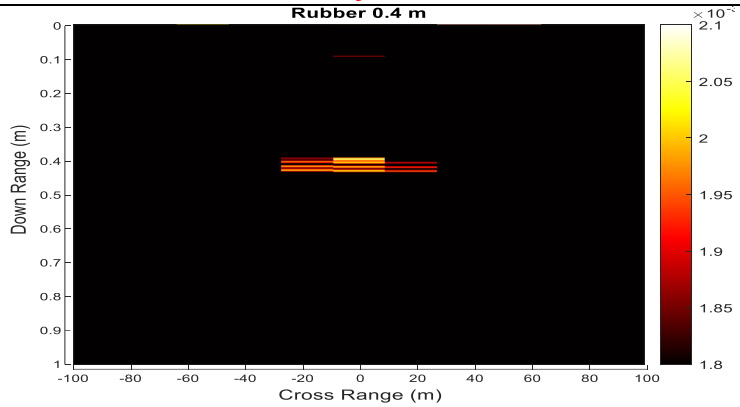

Figure 14. A 2D depicts a rubber target situated 0.4 meters down range behind a wall

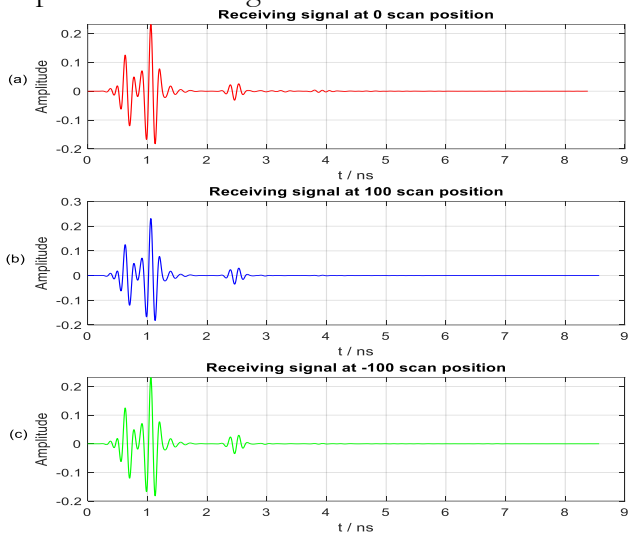

Figure 15. Receiving signals for wood detection at 0.2 m (a) 0 scan position (b) 100 scan position (c) -100 scan position

Figure 14 shows a 2D image of a rubber object located behind a wall at a distance of 0.4 meters. The y-axis represents the downrange where the target becomes visible at the same distance, while the x-axis illustrates the cross-range relative to the antenna's scanning positions. Figure 15(a) analyzes antenna-received signals to detect the presence of an object behind a wall. The signal variations between 0.6 and 1.1 ns correspond to antenna reflections, while those from 2.4 to 2.5 ns are wall reflections. Notably, variations between 3.85 and 3.93 ns indicate reflections from a wood target. Figures 15 (b) and 15 (c) show received signals at scan positions 100 and -100, respectively, revealing only antenna and wall reflections, no scattered object reflections. Figure 16 displays a 2D image of a wood object positioned behind a wall at a distance of 0.2 meters. The y-axis represents the downrange where the target becomes visible at the same distance, while the x-axis depicts the cross-range relative to the scanning antenna positions.

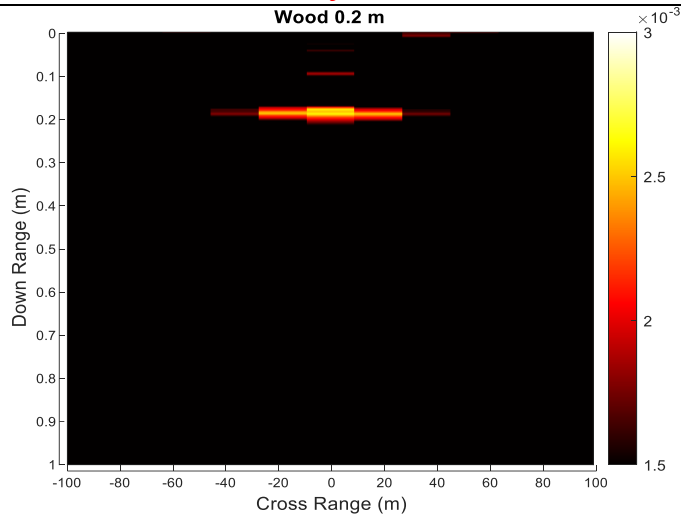

Figure 16. A 2D image depicts a wood target situated 0.2 meters down range behind a wall

Table 3. Comparison of TWI systems based on object size, material, antenna type, number of antenna elements, and wall type

TWI system	Object size	Object Material	Antenna Type	Number of Antenna Elements	Wall Type
[18]	41 x 28 cm	Iron	Vivaldi	2	Concreate
[19]	30 x 45 cm	Metal	Vivaldi	11	Concreate
[20]	45 x 35 cm	Metal	Vivaldi	8	Dry Wall
[21]	30 x 30 cm	Aluminum	Horn	1	Plywood
This work	10 x 10 cm	Rubber, Wood	Antipodal Vivaldi	1	Concrete

Table 3 highlights various TWI systems, showcasing their capability to detect objects of different sizes, materials, and through various wall types using diverse antenna configurations. The first three systems employ Vivaldi antennas, which are known for their wideband performance and high resolution, to detect larger metallic objects like iron and metal. These systems use multiple antenna elements (2, 8, and 11), enhancing their ability to detect larger objects through concrete and drywall. The fourth system uses a horn antenna, with a single element, to detect a smaller aluminum object through plywood. Horn antennas are effective in specific scenarios but may lack the flexibility and compactness offered by other designs. In contrast, the work presented here focuses on detecting significantly smaller objects (10 x 10 cm) made of rubber and wood. This is achieved using a single-element antipodal Vivaldi antenna, a compact and efficient design tailored for smaller, low-reflective materials. The ability to detect such challenging objects through concrete walls, which typically cause high attenuation, underscores the system's advanced performance and optimization. Overall, the table demonstrates a progression in TWI systems, from handling large metallic objects with complex setups to compact, cost-effective solutions capable of detecting smaller, low-contrast objects in demanding environments. This work distinguishes itself by addressing challenging detection scenarios with minimal hardware complexity.

Conclusion:

This study explores signal processing techniques for non-metallic object imaging through walls using a UWB MAVA antenna. The optimized antenna design features stable gain, wide bandwidth, S_{11} below -10 dB, and directional radiation patterns across the 3-10 GHz frequency range. The UWB MAVA antenna was then tested using a wall detection/imaging simulation model for non-metallic targets. The received signals in the time domain were recorded at each scanning position within the through-wall simulation model. By analyzing

received signals in the time domain and applying signal processing methods, small non-metallic targets can be detected and imaged at distances of 0.2 meters and 0.4 meters downrange.

References:

[1] D. S. S. Kaushal, B. Kumar, P. Sharma, "Real time Adaptive Approach for Hidden Targets Shape Identification using through Wall Imaging System," *Def. Sci. J.*, vol. 71, no. 3, pp. 395–402, 2021, doi: 10.14429/dsj.71.16696.

[2] R. Cicchetti *et al.*, "A Microwave Imaging System for the Detection of Targets Hidden behind Dielectric Walls," *2020 33rd Gen. Assem. Sci. Symp. Int. Union Radio Sci. URSI GASS 2020*, Aug. 2020, doi: 10.23919/URSIGASS49373.2020.9232008.

[3] H. Li, G. Cui, L. Kong, S. Guo, and M. Wang, "Scale-Adaptive Human Target Tracking for Through-Wall Imaging Radar," *IEEE Geosci. Remote Sens. Lett.*, vol. 17, no. 8, pp. 1348–1352, Aug. 2020, doi: 10.1109/LGRS.2019.2948629.

[4] K. S. Banavathu Kondalu, Singam Aruna, Naik, "Conformal Lower Edge Corner Defected CPW-fed Elliptical Ring Shaped Antenna for UWB Applications," *Int. J. Microw. Opt. Technol.*, vol. 17, no. 3, pp. 276–284, 2022, [Online]. Available: https://www.researchgate.net/publication/362131083_Conformal_Lower_Edge_Corner_Defected_CPW-fed_Elliptical_Ring_Shaped_Antenna_for_UWB_Applications

[5] and A. Z. N. Alsawaftah, S. El-Abed, S. Dhou, "Microwave Imaging for Early Breast Cancer Detection: Current State, Challenges, and Future Directions," *J. Imaging*, vol. 8, no. 5, p. 123, 2022, doi: https://doi.org/10.3390/jimaging8050123.

[6] A. M. Abbosh, M. E. Bialkowski, M. V. Jacob, and J. Mazierska, "Design of a compact ultra-wideband antenna," *Microw. Opt. Technol. Lett.*, vol. 48, no. 8, pp. 1515–1518, Aug. 2006, doi: 10.1002/MOP.21705.

[7] A. J. P. W. van Verre, F. J. W. Podd, X. Gao, D. J. Daniels, "A Review of Passive and Active Ultra-Wideband Baluns for Use in Ground Penetrating Radar," *Remote Sens*, vol. 13, no. 10, p. 1899, 2021, doi: https://doi.org/10.3390/rs13101899.

[8] A. M. De Oliveira *et al.*, "A Fern Antipodal Vivaldi Antenna for Near-Field Microwave Imaging Medical Applications," *IEEE Trans. Antennas Propag.*, vol. 69, no. 12, pp. 8816–8829, Dec. 2021, doi: 10.1109/TAP.2021.3096942.

[9] V. S. Bhadouria, Z. Akhter, M. J. Akhtar, and P. Munshi, "Automated microwave monitoring of hidden objects for strategic and security applications," *J. Electromagn. Waves Appl.*, vol. 35, no. 18, pp. 2492–2509, Dec. 2021, doi: 10.1080/09205071.2021.1953404.

[10] Y. Rai, S. Gotra, B. Kumar, S. Agarwal, and D. Singh, "A Compact Ultrawideband Antipodal Vivaldi Antenna and Its Efficacy in Through-Wall Imaging," *Sens. Imaging*, vol. 25, no. 1, pp. 1–17, Dec. 2024, doi: 10.1007/S11220-024-00461-W/METRICS.

[11] J. Wang, J. Liu, K. Hou, and Y. Li, "A novel antipodal Vivaldi antenna for ultra-wideband far-field detection," *AEU - Int. J. Electron. Commun.*, vol. 164, p. 154626, May 2023, doi: 10.1016/J.AEUE.2023.154626.

[12] K. P. R. K. Raha, "Through Wall Imaging Radar Antenna with a Focus on Opening New Research Avenues," *Def. Sci. J.*, vol. 71, no. 5, pp. 670–681, 2021, doi: 10.14429/dsj.71.16592.

[13] M. S. S. Sajjad Ahmed, Ariffuddin Joret, Norshidah Katiran, Muhammad Faiz Liew Abdullah, Zahriladha Zakaria, "Ultra-wide band antipodal Vivaldi antenna design using target detection algorithm for detection application," *Bull. Electr. Eng. Informatics*, vol. 12, no. 4, pp. 2165–2172, 2023, doi: https://doi.org/10.11591/eei.v12i4.5081.

[14] J. G. Vera-Dimas, M. Tecpoyotl-Torres, V. Grimalsky, S. V. Koshevaya, and M. Torres-Cisneros, "Analysis of equivalent antennas in RT duroid 5880 and 5870 for GPS operation frequency," *Proc. - 2010 IEEE Electron. Robot. Automot. Mech. Conf. CERMA 2010*, pp. 754–758, 2010, doi: 10.1109/CERMA.2010.133.

[15] H. C. Ba, H. Shirai, and C. D. Ngoc, "Analysis and design of antipodal Vivaldi antenna for UWB applications," *2014 IEEE 5th Int. Conf. Commun. Electron. IEEE ICCE 2014*, pp. 391–394, Oct. 2014, doi: 10.1109/CCE.2014.6916735.

[16] K. Aravinda Reddy, S. Natarajamani, and S. K. Behera, "Antipodal vivaldi antenna UWB antenna with 5.5GHz band-notch characteristics," *2012 Int. Conf. Comput. Electron. Electr. Technol. ICCEET 2012*, pp. 821–824, 2012, doi: 10.1109/ICCEET.2012.6203866.

[17] A. S. D. and S. Kumar, "A Survey of Performance Enhancement Techniques of Antipodal Vivaldi Antenna," *IEEE Access*, vol. 8, pp. 45774–45796, 2020, doi: 10.1109/ACCESS.2020.2977167.

[18] C. R. P. Dionisio, S. Tavares, M. Perotoni, and S. Kofuji, "Experiments on through-wall imaging using ultra wideband radar," *Microw. Opt. Technol. Lett.*, vol. 54, no. 2, pp. 339–344, Feb. 2012, doi: 10.1002/MOP.26543.

[19] O. T. Stefano Pisa, Renato Cicchetti, Emanuele Piuzzi, "A Comparison between Multiple-Input Multiple-Output and Multiple-Input Single-Output Radar Configurations for Through-the-Wall Imaging Applications," *Int. J. Antennas Propag*, 2022, doi: https://doi.org/10.1155/2022/3887314.

[20] Y. Wang, Y. Yang, and A. E. Fathy, "Ultra-wideband vivaldi arrays for see-through-wall imaging radar applications," *IEEE Antennas Propag. Soc. AP-S Int. Symp.*, 2009, doi: 10.1109/APS.2009.5172292.

[21] M. J. N. R Chandra, Abhay N Gaikwad, Dharmendra Singh, "An approach to remove the clutter and detect the target for ultra-wideband through-wall imaging," *J. Geophys. Eng.*, vol. 5, no. 4, pp. 412–419, 2008, doi: https://doi.org/10.1088/1742-2132/5/4/005.